

## HALO STATISTICS ANALYSIS WITHIN MEDIUM VOLUME COSMOLOGICAL N-BODY SIMULATION

N. Martinović

Astronomical Observatory, Volgina 7, 11060 Belgrade 38, Serbia

E-mail: nmartinovic@aob.rs

(Received: August 19, 2014; Accepted: January 9, 2015)

**SUMMARY:** In this paper we present halo statistics analysis of a  $\Lambda$ CDM N-body cosmological simulation (from first halo formation until  $z = 0$ ). We study mean major merger rate as a function of time, where for time we consider both per redshift and per Gyr dependence. For latter we find that it scales as the well known power law  $(1 + z)^n$  for which we obtain  $n = 2.4$ . The halo mass function and halo growth function are derived and compared both with analytical and empirical fits. We analyse halo growth through out entire simulation, making it possible to continuously monitor evolution of halo number density within given mass ranges. The halo formation redshift is studied exploring possibility for a new simple preliminary analysis during the simulation run. Visualization of the simulation is portrayed as well. At redshifts  $z = 0 - 7$  halos from simulation have good statistics for further analysis especially in mass range of  $10^{11} - 10^{14} M_\odot/h$ .

**Key words.** dark matter – galaxies: halos – large-scale structure of Universe – methods: numerical

### 1. INTRODUCTION

Current dominant cosmological paradigm is  $\Lambda$ CDM - cold dark matter coupled with dark energy ( $\Lambda$ ) (see e.g. Planck Collaboration 2013, Lahav and Liddle 2014, etc.). Within that paradigm (as within every other cosmological paradigm) one of the major assignments is to determine formation and evolution of large scale structures. Although there is a tendency to find analytical solutions, reaching them is still beyond the scope of current apparatus. Thus, numerical simulations are one of the essential tools for probing structure formation (Springel et al. 2006).

From the ingenious work of Holmberg in 1941 (galaxy collision simulated with light bulbs) and pioneering simulations by von Hoerner (1963), Aarseth (1963), Peebles (1970) and White (1976), rise in com-

puter power has driven advances in computational astrophysics (Dehnen and Read 2011). At present time, together with deep field observations and large data surveys, cosmological simulations are irreplaceable part of new era of precision cosmology. They are used for large scale structure evolution (Millennium - Springel et al 2005, Millennium II - Boylan-Kolchin et al. 2009, Teyssier et al. 2009, Kim et al. 2011, Millennium XXL - Angulo et al. 2012, etc.), near-field cosmology research (CLUES project - for example: Gottloeber et al. 2010), and for galaxy evolution (ILLUSTRIS - Vogelsberger et al. 2014). Increasing mass resolution makes it possible to study evolution of halos in greater details as it resolves morphology and adds constraints to what simulations need to reproduce to match observations. Statistics obtained from connection of observations, theory, and simulations will be used to test our simulation as well.

Most of matter in the universe is dark and is initially smoothly distributed (White 1994). From simulations we see that from this quasi smooth distribution, evolve array of sheets, filaments and clusters named cosmic web (Bond et al. 1996). Constituents of these structures are in the form of dark matter halos: virialized dense clumps of dark matter (Cooray and Sheth 2002). Considering that halos represent potential wells into which matter falls in, it is assumed that galaxies form and evolve within them (White and Rees 1978). More interestingly, understanding evolution of underlying dark matter density field represented by dark matter halos can help us to interpret clustering of galaxies (Kauffmann et al. 1999). Of course, these halos and their properties are result of numerical simulations.

There are two ways we can study halos: we can study distribution of halos, and we can study their internal structure (Harker et al. 2006). Distribution, which will be of more interest to us in this paper, is an important tracer for evolution of halos and, thus, structure growth (e.g. Lukić 2008). Furthermore, within numerical simulations we are given an opportunity to study assembly and growth of the halos. By following temporal evolution of the halo and their statistical characteristics (growth, clustering, formation times, etc), we can expand our knowledge on evolution of galaxies that reside within them. Structure in which we follow evolution of halos from small clumps to large objects is referenced to as the merger tree (Kauffmann and White 1993, Lacey and Cole 1993.).

One of the widespread halo distribution analysis is the halo mass function, precisely due to its importance in connection between the dark halo and galaxy properties. Also it is a very useful tool for analysis and testing of numerical simulations. It is sensitive to cosmological parameters (Lukić 2008). With it, for example, it can be seen that for WDM (warm dark matter) cosmologies it is predicted that there are fewer halos of lower mass than what is predicted with the CDM (cold dark matter) counterpart (Colin et al 2000, Angulo et al. 2013).

In this paper we will present the medium volume pure cosmological simulation that we have performed. Through halo catalogues and merger tree we will study general halo characteristics. Apart from considerations of major merger rate from simulation (Gottloeber et al. 2001, Fakhouri and Ma 2008, Angulo et al. 2009, Wetzel et al. 2009, Genel et al. 2009, Fakhouri et al. 2010, Hopkins et al. 2010), we will concentrate on the formation redshift of halos showing tendency, as predicted by bottom-up mode of structure formation, toward massive halos being formed later in the life of Universe. We will address a possibility for the new approach on using a simple formation redshift analysis (hence requiring less computing resources) as a mean for preliminary analysis of halo formation during the simulation run.

We will compare halo mass function of our halos with both analytical and empirical fits, showing evolution of understanding of halo formation, starting from spherical collapse of Press and Schechter (1974), through elliptical correction of Sheth, Mo

and Tormen (2001), continuing with the refinement done by numerical simulations of Warren et al. (2006) and Angulo et al. (2012).

Alternative path for general halo distribution and characteristics analysis will be presented in the form of halo growth function (Heitmann et al. 2006). We derive the halo growth function both for all the related analytical and empirical fits and for our simulation, thus allowing us to easily analyze the evolution of halo number density with a very good time resolution within the used mass bins.

We will show that the analysis of our halo distribution characteristics is in good agreement with analytical fits and other simulations. This simulation will be used as a platform for subsequent research.

This paper is organized as follows. In Section 2. the initial conditions of our simulation are presented. In Section 3. the attributes of used computational resources can be found. The software used for acquiring halo catalogues and creating merger tree of our simulation is presented in Section 4. Implemented analysis is presented in Section 5 with focus on the mass function in subsection 5.1 and halo growth function in subsection 5.2. Results are detailed in Section 6 with a short overview of visualization of halos. In Section 7 we engage in discussion and at the end of that section, short concluding remarks are presented.

Convention used for presenting Hubble constant in this paper is:  $H = 100 h \frac{\text{km}}{\text{s Mpc}}$ .

## 2. INITIAL CONDITIONS

For initial conditions we have used Las Damas cosmology (McBride et al. 2009) which assumes flat space and cosmological parameters with values:  $\Omega_m = 0.25$ ,  $\Omega_\Lambda = 0.75$ ,  $\Omega_b = 0.04$ ,  $h = 0.7$ . For the initial power spectrum, code CMBfast (Seljak and Zaldarriaga 1996) was used, with power-law index  $n_s = 1$  for primordial power spectrum and  $\sigma_8 = 0.8$ , which is the mean linear mass fluctuation in spheres of radius of 8 Mpc/h extrapolated at  $z = 0$ .

The linear expansion part of the simulation was computed from the perturbed density field using the 2nd order Lagrangian perturbation theory (Crocce et al. 2006) up to  $z = 599$ . The non-linear part of the simulation was calculated using the publicly available, highly parallelized, Tree-PM N-body code GADGET2 (Springel 2005) that uses the hierarchical tree for calculations of short-range forces and particle-mesh algorithm for calculations of long-range forces. The simulation was run up to the present time ( $a = 1$ ) in a periodic box with size of 130 Mpc/h, employing  $512^3$  dark matter particles and a comoving softening length of 8 kpc. Particle mass resolution is  $1.14 * 10^9 M_\odot/h$ .

Large box suppressing finite volume artifacts and high initial redshift of the simulation provide accurate results for acquiring mass function (Lukić et al. 2007). Generally, both things are tuned toward reduction of systematic effects.

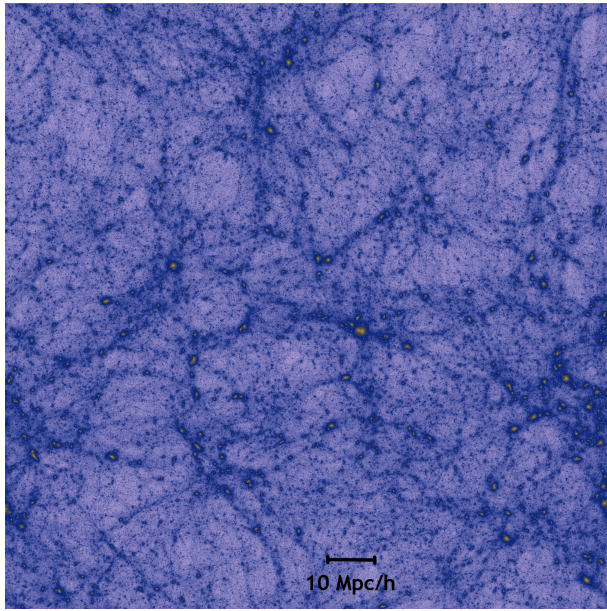


**Fig. 1.** False color visualization of final snapshot ( $z \sim 0$ ). All particles are collapsed along one axis, projecting 3D box onto 2D representation. Brighter colors mark denser regions.

Simulation was run with a grid structure that leaves possibility to zoom in resimulations up to mass resolution of  $2048^3$ . In total there are 84 snapshots taken during the simulation, starting with 6 snapshots between redshifts 599 and 9 ( $z = [499, 249, 149, 99, 49, 19]$ ) and the rest from the redshift 9 till the present time in the multiples of 1.0304106 (in the scale factor space). Each snapshot is approximately 3.5 GB and all are available for further analysis.<sup>1</sup> Visualization of final snapshot is given in Fig. 1.

### 3. COMPUTING RESOURCES

Simulation was executed in PARADOX Cluster at Scientific Computing Laboratory of Institute of Physics Belgrade. Cluster consists of 89 worker nodes powered by 2 x quad core Xeon E5345 @ 2.33 GHz and each with 8GB of RAM. Computing nodes are interconnected with the Gigabit Ethernet network. Total available storage is up to 50TB. For the simulation we have used 256 cores running about 39000 hours in total computing time (152 hours per processor) with 34000 timesteps. Adaptive time-step calculations were used when necessary for individual particles.

### 4. HALO CATALOGUES AND MERGER TREE

Analyses involving halos require that we first identify a halo, and then determine its mass (Lukić et al. 2007)

The formalism for identification of halos was first introduced by Press and Schechter (1974) by assuming spherical collapse. They identified density peaks in matter distribution and then added particles in layers around the center of the peaks until the mean density within the particular sphere reaches the theoretically derived density threshold.

Another approach, called friends-of-friends, was developed by Davies et al. (1985). They defined the halo by assuming that particles are bound together if each of them is within a predefined linking length from at least one other particle in that group.

For creation of the halo catalogue we have used the halo finding software named ROCKSTAR (Behroozi et al. 2013a). Its primary focus is on consistent accuracy over many timesteps. It works by combining friends-of-friends (FOF), phase-space, and spherical overdensity analysis in locating halos. The analysis is started by classical 3D FOF algorithm (with large linking length,  $b = 0.28$ ), and subsequent 6D iterations where the FOF hierarchy is established (by choosing that 70% of the group's particles are linked iteratively in subgroups).

From those substructures halos are formed by placing seeds in deepest substructures in hierarchy, after which particles are recursively assigned to the closest seeds based on their phase-space vicinity. This is repeated for all levels of the hierarchy. Then it uses the information from previous snapshots to establish halo/subhalo connections. Tree code is used to find the halo density peaks after which it unbounds the non-virialized particles. Unbinding is done by calculating full particle potentials after which halo masses and spherical overdensity are calculated following the rest of the halo properties as well. The virial overdensity is defined by using the definition of  $\rho_{\text{vir}}$  from Bryan and Norman (1998), which corresponds to 360 times the average matter overdensity (which is  $\rho_m = \Omega_m \rho_{\text{crit}}$ ). So, within the virial radius of the halo, the density of matter is equal or higher than the virial overdensity.

We have used minimum of 100 particles as a lower limit for a halo, with the FOF linking length set  $b = 0.28$  and the FOF linking fraction set to 0.7, both recommended settings. With such limits the first structures were discerned by ROCKSTAR on snapshot which corresponds to redshift 9 (scale factor 0.1). Total number of found halos is over 66000 at redshift 0.

Merger tree was assembled using Consistent Merger Tree (Behroozi et al. 2013b), a software package that is complementary with the ROCKSTAR halo finder and which is designed so that for halo properties, dynamical consistency is ensured across timesteps.

<sup>1</sup>Contact author for the full free and open access to snapshots, and/or halo catalogue, etc.

If one or more particles of a halo identified in a snapshot become a gravitationally bound part of a single halo in a following snapshot then such an interaction is declared a merger. Interacting halos are declared progenitors and a resulting halo is called a descendant. Mergers are considered to be major when the descendant halo has progenitors whose mass ratio is  $> 0.3$ . Both halo and subhalo mergers are considered.

## 5. ANALYSIS

Apart from allowing us a simple analysis such as total number of halos through time, halo catalogues and merger tree can be used for analysis of many other characteristics of cosmological simulations.

One of the first analysis was done by determining the total number density of halos in our simulation across all redshifts. From our halo catalogue we simply extract the number of halos per redshift and divide it by volume. This will give us a brief view of the first appearance of halos and change in their total number.

As major mergers are the essential part of many important events in the Universe, they are usually the focus of analysis. We defined them as mergers where the ratio of halo masses involved (that are coalescing) is above 0.3. We use the merger tree of our simulation to derive the number of major mergers over number of all halos of same population both per unit of Gyr and per unit of redshift independently. We also use the merger tree to extract the number of major merger events and trace their number density through our simulation time. Both halo and subhalo mergers are taken into consideration.

Another interesting thing that can be discerned from the merger tree is the mean formation time of halos at redshift 0 (Lacey and Cole 1993) in certain mass bins since we have the information on how the halos evolve through time. It is derived by binning halos according to mass on redshift 0, and then searching for the mean redshift when the main progenitor mass was half of the mass at the final redshift.

We have performed a complementary analysis of identification of the highest mass halo within one snapshot which effectively identify when the first halos of certain mass appear in our simulation, and it points to possible significant merger events. This analysis can be done for each snapshot as it is retrieved, thus revealing where more extensive analysis should be performed.

These analyses paint the picture of structure formation by exploring the halo evolution. For further halo statistics we will turn to the halo mass function analysis and halo growth function.

### 5.1. Mass Function

The halo mass function is defined as number of halos per volume of space, per unit of mass. We treat the mass function as represented in Lukić et al. (2007). Usually halos are binned together according

to mass or mass logarithms and for each bin (comoving) the number density is determined, in our case, we have chosen the latter case. Bins are selected in such a way that they contain a significant population of halos, thus reducing the shot noise due to low population in each bin.

In the case of our halo mass function, halo bins of width  $\Delta \log M = 0.5$  dex were chosen, where from hereafter  $\text{dex} = \Delta \log(M / (M_\odot/h))$ , and each data point represents the center of its respective mass bin.

So, for our mass logarithms, the mass function can be represented as:

$$F(M, z) = \frac{dn}{d \log M}. \quad (1)$$

Apart from calculating the halo mass function from simulations, we can estimate how it would look from:

$$F(M, z)_{\text{analy}} = \frac{\rho_0}{M} f(\sigma) \left| \frac{d \ln \sigma}{d \log M} \right|; \quad (2)$$

where  $f(\sigma)$  represents various analytical and empirical solutions for the mass function,  $\sigma$  is the mass variance of linear density field and  $\rho_0$  is the mean density of the Universe. Generally,  $f(\sigma)$  is considered not directly linked to the redshift, that is, the redshift dependence is gained through  $\sigma(M, z)$ , where it is achieved through the growth factor (Murray et al. 2013). The mass variance is also sensitive to different cosmologies.

For calculation of mass variance, the power spectrum, transfer function, top hat function the same method that is described in Murray et al. (2013) was used. The transfer function was calculated by using the CMBfast code. As showed in Murray et al. (2013), the mass variance was calculated using the top-hat filter, the linear power spectrum is used and the redshift dependence of fitting functions was achieved through the mass variance, or more precisely, through its connection to the growth factor which is governed by the redshift dependence.

Historically, the first analytical model of the mass function was developed by Press and Schechter (1974) (PS). Although finer fits were developed in the meantime, especially for higher redshifts, the PS formalism has a good agreement in lower redshifts ( $z \rightarrow 0$ ) and it is a good starting point. It assumes that the entire mass is in halos and it considers a purely spherical collapse. It was shown later that it generally overestimates the number of lower mass halos and underestimates the number of high mass halos. Function is given as:

$$f_{\text{PS}}(\sigma) = \sqrt{\frac{2}{\pi}} \frac{\delta_c}{\sigma} \exp\left(-\frac{\delta_c^2}{2\sigma^2}\right), \quad (3)$$

where  $\delta_c = 1.686$  is the critical value of density perturbation (overdensity) of a dark matter sphere after which it collapses into a virialized halo, and  $\sigma$  is the mass variance, same as earlier.

Improvement over PS was done by Sheth, Mo and Tormen (2001) (SMT, hereafter). They extended the PS fit with an elliptical collapse model. Basically, they theoretically derived a fit that showed less discrepancy from mass functions calculated directly from numerical simulations. Their function is given as:

$$f_{\text{SMT}}(\sigma) = A \sqrt{\frac{2a}{\pi}} \left[ 1 + \left( \frac{\sigma^2}{a\delta_c^2} \right)^p \right] \frac{\delta_c}{\sigma} \exp \left[ -\frac{a\delta_c^2}{2\sigma^2} \right], \quad (4)$$

where  $A = 0.3222$ ,  $a = 0.707$  and  $p = 0.3$ , and  $\delta_c = 1.686$ . Interestingly, if we set:  $A = 0.5$ ,  $a = 1$  and  $p = 0$  we would get PS from the above formula.

Another very interesting halo mass function fit was developed by Warren et al. (2006) (Warren, hereafter). We focused on it, apart from PS and SMT, because Warren computed their fit by using a large number of cosmological simulations using the same code and the same cosmology with statistics spanning same mass range as we did in our simulation. Warren function is represented as:

$$f_w(\sigma) = 0.7234 (\sigma^{-1.625} + 0.2538) \exp \left[ \frac{-1.1982}{\sigma^2} \right]. \quad (5)$$

Last halo mass function fit we used for comparison was derived by Angulo et al. (2012). It is derived from unprecedented cosmological simulation that uses  $6720^3$  particles representing dark matter structures in a periodic box of size 3 Gpc/h, thus allowing within the same simulation, to span even a greater mass range than Warren's fit. It is given as:

$$f_A(\sigma) = A \left[ \left( \frac{b}{\sigma} \right)^a + 1 \right] \exp \left[ -\frac{c}{\sigma^2} \right], \quad (6)$$

where  $A = 0.201$ ,  $a = 1.7$ ,  $b = 2.08$ , and  $c = 1.172$ .

## 5.2. Halo growth function

Another path of analyzing the halo statistics over the course of simulation was done by analyzing the halo growth function (Heitmann et al. 2006). It is defined as the number of halos in given mass bins throughout the simulation. From it we can analyze how mass is distributed over halos through time. For that we extend our halo growth function over all available snapshots, giving us a finer time resolution and making the analysis more continuous. We are using it to focus more on how the abundance of halos within one mass bin is evolving through time and to get an insight into changing the ratio of these bins at different redshifts.

For construction of a halo growth function we have chosen wide logarithmic mass bins considering that population of each bin varies across redshifts. Wide mass bins enable us to keep the number of low populated data points to minimum, considering that within a short period of time, the population number of each bin rises to a significant level. On the

other hand, we still have enough information from these bins to analyze the evolution of number density of low and high mass halos throughout the simulation. Four bins covering masses from  $10^{11} M_\odot/h$  to  $10^{15} M_\odot/h$  were selected.

We derive an estimation of the halo growth function by integrating the mass function for given mass bins over redshifts:

$$n(M_1, M_2, z) = \int_{M_1}^{M_2} F(M, z) d \log M \quad (7)$$

here  $n(M_1, M_2, z)$  is the number density of halos in a mass bin limited by  $M_1, M_2$  on a redshift  $z$  for a given fit  $f(\sigma)$  on which  $F(M, z)$  is dependent, as seen in Eq. (1).

## 6. RESULTS

The number density of halos across all masses as a function of redshift in our simulation is represented in Fig. 2. Each point represents the total number density of dark matter halos in one snapshot. As the simulation progresses and dark matter starts to form more dark matter halos we see a rise in their number density. Having in mind that our halo catalogue has halos above  $10^{11} M_\odot/h$ , we see that the total number density is starting to decrease as the simulation approaches lower redshifts (toward  $z \sim 0$ ).

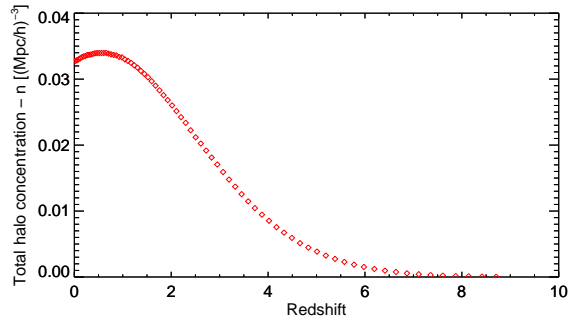


**Fig. 2.** The total number density of identified halos in the simulation as a function of redshifts. We see gradual formation of dark matter halos and subsequent reduction of their number density toward  $z \sim 0$ .

Major mergers, presented in Fig. 3, are considered as another interesting analysis.

Top of Fig. 3 is a graph with two distinct plots, both plotted as a function of redshift, where we track merger rate of halos of mass greater than  $10^{12} M_\odot/h$  per unit of Gyr,  $dN_{\text{merge}}/dt$  (blue x); and per unit of redshift,  $dN_{\text{merge}}/dz$  (red diamonds). Halos with mass greater than  $10^{12} M_\odot/h$  are chosen because this enables us to compare our results with wide a range of previous results. As seen, both plots

cover the same halos over the same time, but the difference is, as noted in Fakhouri and Ma (2008), that the mean merger rate per Gyr increases with redshift contrary to the mean merger rate per redshift which is constant. This is due to the cosmological factor,  $dt/dz$ , spanning shorter times at higher redshifts.

The black line is a power law fit (Genel et al. 2009) showing that mean merger rate per Gyr increases with redshift as  $\propto (1+z)^n$ , where we find  $n = 2.4$  for the plot shown. Black asterisks represent results from Gottloeber et al. (2001), where they consider the major merger rate for primary halos only. Two nearly horizontal dotted lines are results for the major merger rate from the Millennium simulation from Fakhouri and Ma (2008, brown, upper line) and from Angulo et al. (2009, green, lower line).

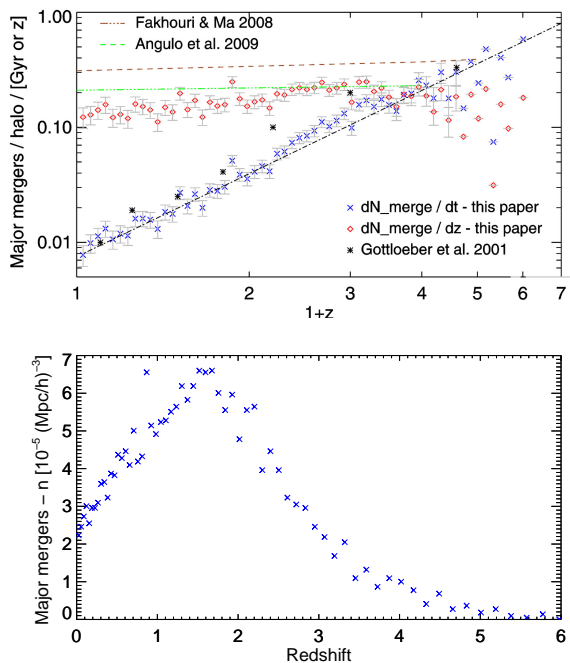


**Fig. 3.** *Top:* Mean merger rate as a function of redshift. Red diamonds are per redshift dependence, results of Fakhouri and Ma (2008) are presented as brown dotted line and Angulo et al. (2009) results are presented as green dotted line. Blue crosses are per Gyr dependence, overplotted are black asterisks which represent results of Gottloeber et al. 2001. As can be seen, the mean major merger per redshift is nearly constant, while per Gyr changes as  $\propto (1+z)^n$  with  $n = 2.4$  (black line). Error bars are Poisson standard errors. Error bars for the right-most points are large and are omitted. *Bottom:* Number density of major mergers as a function of redshift. Derived by counting the number of a new major merger events from each snapshot normalized to the number of identified halos in the snapshot. A clear peak is seen around  $z \sim 2$  which coincides with the maximum quasar abundance.

The bottom graph in Fig. 3 is a total number density of major mergers in our simulation as a function of redshift. Points represent the major merger number density from each snapshot. They have been derived by counting the number of a new major merger events for each snapshot (that is descendants which had progenitors merging from previous snapshot) normalized to the total number of identified halos per snapshot. It can be noted that the number density of major mergers has the same trends as the total number density of identified halos. We see the rise in number density as more dark matter halos are created and become dynamically involved and its subsequent receding when the dark matter halo pairs with similar mass become sparse. Calculated values of plotted number density are obviously smaller due to lesser frequency of major mergers per volume (in comparison to the total halo number density, for example), but a clear peak can be seen as well.

In Fig. 4 we see two plots in connection to the formation time. The first one, labeled by red diamonds, displays the redshift of the first appearance of halos as a function of halo mass. We introduce it as a new way for a simple preliminary analysis of halo formation during cosmological runs. It is a simple visualization of the highest mass halos from each snapshot. We see practically a linear trend of constantly higher mass halos as the simulation was progressing. Points that are spread horizontally, i.e. the ones that point to the high mass gain for halo at the next snapshot, suggest a significant merger event, making this analysis inexpensive precursor of the merger tree. Also, it should be considered that this plot considers only a single, the most massive, halo from each snapshot.

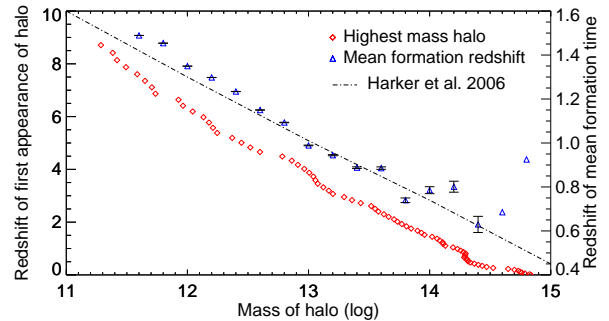


**Fig. 4.** – Redshift of the first appearance of halos as a function of halo mass (red diamond, left y-axis). Within this plot we visualize mass of the highest mass halos in each snapshot of simulation. The other curve is the mean formation time redshift as a function of halo mass bins (blue triangle, right axis). From both we see that bigger halos identified at  $z \sim 0$  tend to form earlier in the simulation. Black dotted line represents results of mean formation redshift from the Millennium simulation as presented in Harker et al. (2006). Error bars are Poisson standard errors. At largest halo masses, we omit last two mass bins because of the numerical noise due to the small halo population at these masses.

The second plot (blue triangles) is the mean formation time redshift as a function of halo mass bins. It represents the mean value of redshift at which the most massive progenitors of a halo from redshift 0 have half of their mass. In fact, that gives us average redshift at which all the halos of certain mass bin will form. The mass bin covers ranges from  $10^{11}$  to  $10^{15} M_{\odot}/h$ , has width of 0.2 dex and is represented by blue triangles positioned at the center of the bin range. From this we can see that it is linear (apart for bins with the highest mass), indi-

cating that massive halos from  $z \sim 0$  tend to form later in the simulation (closer to  $z \sim 0$ ). It should be noted that the highest mass range in the mean formation time plot is stricken by the low population of those bins heavily affecting averaging. The dotted line in the plot represents the empirical fit for the mean formation time of halos from the Millennium simulation as seen in Harker et al. (2006). It can be noted that the mean formation times for halos in both simulations are in a good agreement.

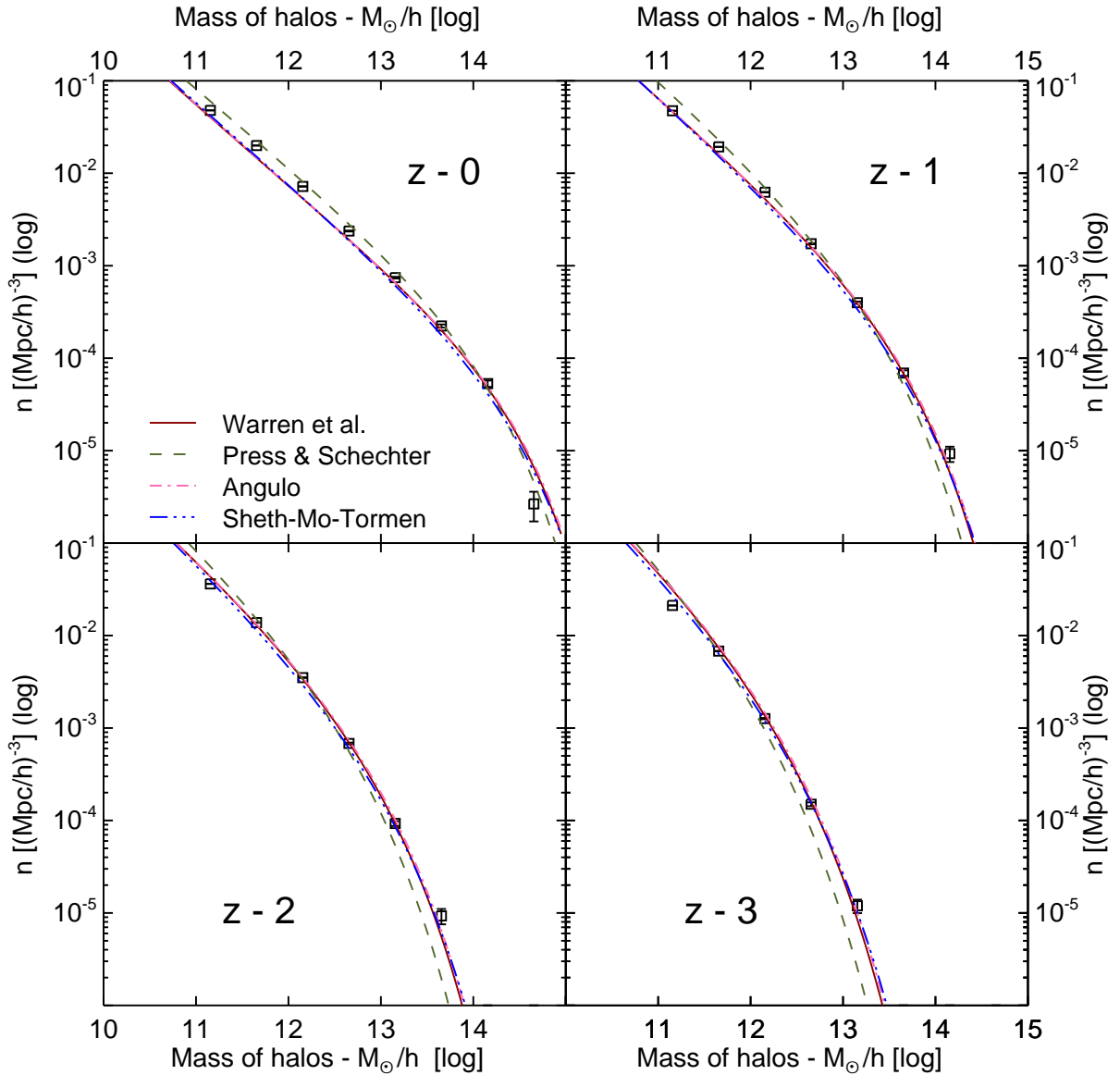


**Fig. 5.** Plot of mass function: the number density of halos as a function of halo mass (binned), plotted for 4 different redshifts ( $z \sim 0, 1, 2$  and  $3$ ). Squares represent centers of mass bins of width 0.5 dex. Results from simulation are compared with 4 different fits, 2 analytical: Press-Schechter (1974); Sheth, Mo and Tormen (2001); and 2 empirical: Warren et al. (2006) and Angulo et al. (2012). We see a good agreement between the simulation and most of the fits within each redshift, especially  $z \sim 1$  and  $z \sim 2$ . The Press-Schechter fit shows a significant divergence at higher redshifts. Fewer number of squares in the  $z \sim 4$  plot is a consequence of massive halos not yet formed. Error bars are the Poisson standard errors.

After computing the halo mass function from our simulation as represented by Eq. (1), we compare it to several known analytical and empirical solutions of interest. In Fig. 5 we can see the halo mass function calculated from the executed simulation at 4 different redshifts, ( $z \simeq 0, 1, 2$  and  $3$ ) with analytical fits overplotted as lines. Analytical and empirical fits can cover a wider mass range, but we have restricted it to  $10^{10}$  to  $10^{15} M_{\odot}/h$  to coincide with the mass range available from the simulation. Squares represent centers of mass bins used to bin the halo masses found in our halo catalogue, where bins have width 0.5 dex. As can be seen, there are less squares available at higher redshifts, because higher mass dark matter halos have not formed yet at those redshifts. It can be noticed that there is a good agreement between fits at all redshifts except for the Press-Schechter fit which diverges both at high and low mass ranges and across all redshifts. A good agreement between the simulation and other fits (except PS as noted) is also noticeable with only a slight disagreement between the highest mass bins at redshift 0, but as mentioned earlier, that can be due to the lower number of halos within the bin.

In Fig. 6 the halo growth function for our simulation is given against analytical and empirical expectations. It represents the number density of halos within a certain bin as a function of redshift. The same fits used for halo mass function are presented here with overplotted points derived from our simulation. It is clear that results are distributed within 4 mass bins covering masses of  $10^{11} - 10^{15} M_{\odot}/h$  spanning the entire simulation period in which the halos were identified. Using this plot we can determine red-

shifts around which halos of certain mass bin begin to form (except for the lowest mass bin). Again, we notice a discrepancy between the Press-Schechter fit over other fits, amplified at higher redshifts. Moreover, we see that at high redshifts all fits diverge to some extent. A good agreement at lower redshift ( $0 < z < 1$ ) between the simulation results and fits is noticeable across all mass bins, but at higher redshifts, some divergence appears. For the highest mass bins there is an overabundance of halos at  $z > 1$  but, as seen from other analysis, this is most likely due to a low number of halos populating mass bins at those redshifts. The same problem affects other mass bins near their maximum redshifts.

If we compare fits and results for different mass bins in Fig. 6, it becomes clear that mass bins with higher masses emerge later in the simulation, thus once again stressing the fact that higher mass dark matter halos form later.

Visualization of data has been performed both for popularization purposes and for testing the integrity of the halo finder. In Fig. 1, visualization of the final snapshot can be seen. Along with other snapshots it has been performed by collapsing all particles along one axis, leaving two dimensional distribution of particles. After that, the density was calculated by simple binning of particles, where finally, the color was assigned proportionally to density (darker color to low density, brighter colors to high density regions). For animation purposes particle positions were extrapolated in between snapshots in order to lengthen the animation for easier apprehension of events within it.

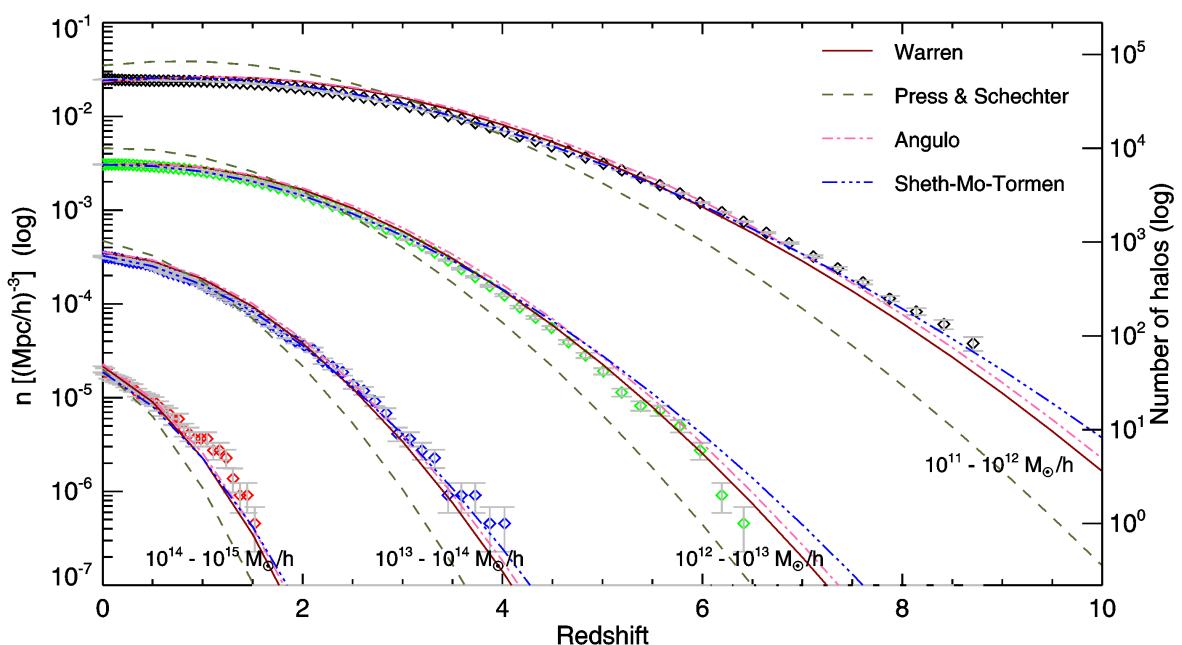


**Fig. 6.** Plot of halo growth functions: number density of halos as a function of redshift presented for 4 mass bins. Results of simulation are compared to 4 different fits, same ones that were used in halo mass function analysis, presented in Fig. 5. A good agreement at lower redshift ( $0 < z < 1$ ) between the simulation results and fits is noticeable across all mass bins, but at higher redshifts, some divergence appears. Note the discrepancy between fits themselves at higher redshifts. Error bars are the Poisson standard errors.

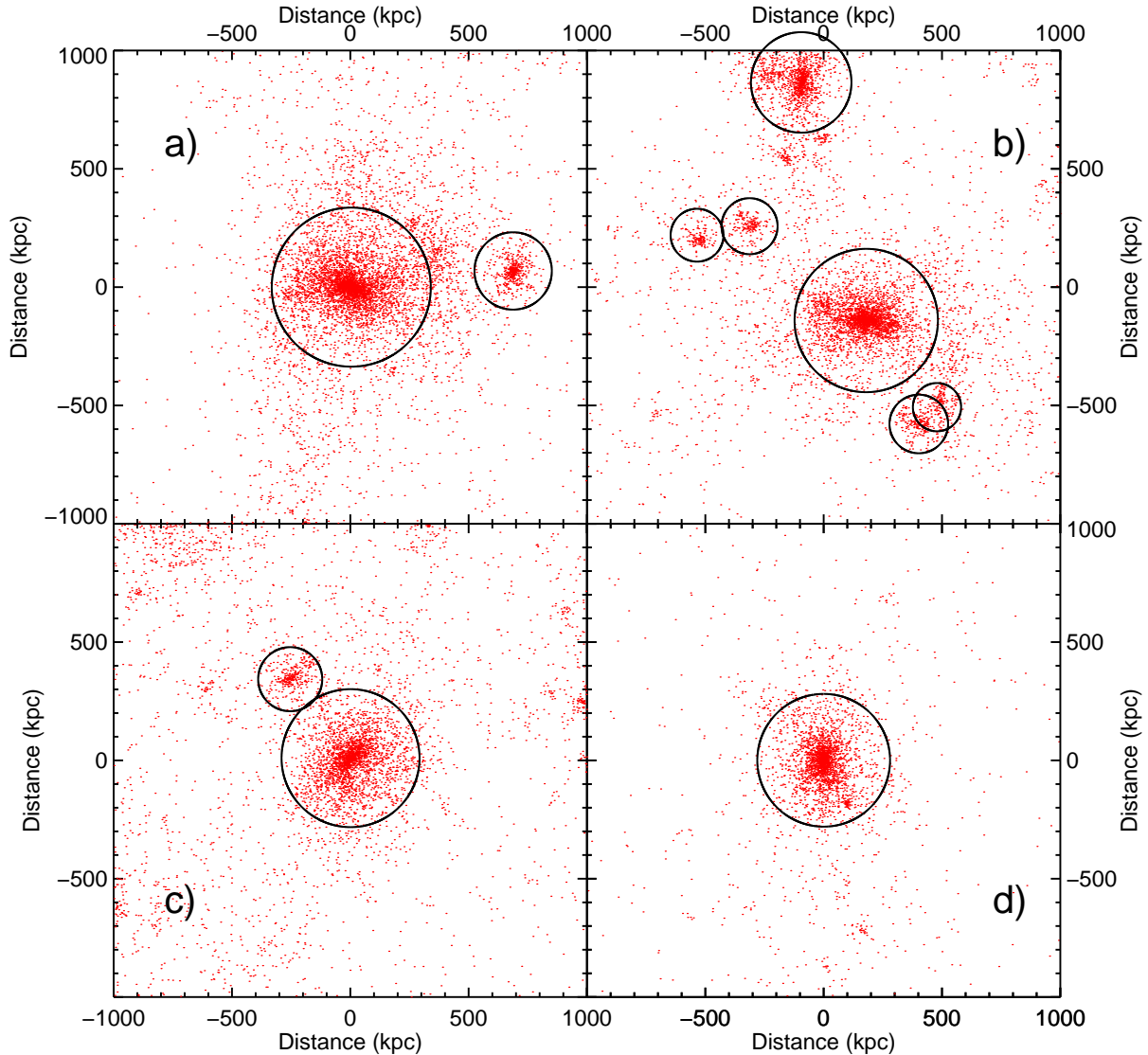


**Fig. 7.** Visualization of several identified dark matter halos from simulation. Black circles represent the virial radius of identified halos from the halo finder. Note the different density and ellipticity of halos.

In Fig. 7, visualization of distinct halos is presented. We have chosen halos that cover a wide range of properties (isolated, in clusters, etc) to visually confirm the halo finder results. For each halo a 3D box around it was extracted and visualization was done by simply plotting particle positions sliced on one axis through the derived center of a halo. Overplotted are the circles representing the virial radius of identified halos from the halo finder. It can be seen that there is no major discrepancies between the halo finder identified halos and the visual representation of them.

## 7. DISCUSSION AND CONCLUSION

In this paper we present results of pure N-body cosmological simulation of  $130 \text{ Mpc}/h$  periodic box with  $512^3$  particles performed with GADGET2. The halo catalogue and merger tree were obtained using the ROCKSTAR code and through their analysis the dark matter halo distribution statistics is presented. Visualization of simulation was described and depicted. Special consideration was dedicated to halo formation time, major merger rate, mass function and halo growth function which were derived with good time resolution and compared with both analytical and empirical fits.

A quick look at total number density of halos across all redshifts tells us that we have an initial rise in number of halos and that after certain redshift their number starts to recede, which is expected.

The merger tree gives us, among other things, insight into major mergers of our simulation. If we concentrate on the mean merger rate per time plots we notice that we have a good agreement between our plot and that of Gottloeber et al. (2001) who consider the primary halo major mergers (consistent with our masses of more than  $10^{12} M_{\odot}/h$ ), but there is a discrepancy between our results and major mergers of Millennium simulations (Fakhouri and Ma 2008, Fakhouri et al. 2010) where they consider only the halo-halo mergers, while in our case, as already mentioned, the subhalo mergers are considered as well. It should also be noted that our simulation has a lower statistical sample and a finer time resolution, leading to lower number of major mergers at each point. The dependence on time resolution was shown by Gottloeber et al. (2001) where, as expected, the scatter increases with finer resolution i.e. plots consist of more points that are less populated. Scatter due to low population is obvious for higher redshifts in our sample simply because the first halos of considered mass did not appear until  $z \sim 6$  meaning that the number of major mergers is low around that redshift.

Angulo et al. (2009) have used the Millennium simulation ( $> 10^{12} M_{\odot}/h$ ) in the same mass range as us and with the same considerations for mergers (subhalo mergers as well). Their results are in a better agreement with our results than that of Fakhouri and Ma (2008), but still with slight offset. Considering the already mentioned discrepancies with Fakhouri and Ma (2008) also from Millennium simulation, this points us to work of Hopkins et al. (2010). They tried to quantify the contribution of uncertainties and systematic effects for different means of deriving merger rates and they came to the conclusion that there is a discrepancy of factor  $\sim 2 - 3$  for high-resolution dark matter simulations if mergers are defined consistently (within the same cosmology).

Another test for validity of our merger rate came from Genel et al. (2009) from which we used the fitting function, compared it with our mean merger rate per Gyr and found that it scales with redshift as a power law  $\propto (1+z)^n$ , where we found that  $n$  fits our data well if  $n = 2.4$ . This rate coincides with the form of power law acquired from observations for scaling merger rates with redshift for:  $n = 2.43$  (Bridge et al. 2009),  $n = 2.5$  (Burkey et al. 1994),  $n = 2.3$  (Patton et al. 2002),  $n = 2.7$  (Le Fevre et al. 2000).

Looking at the plot that deals with total number of major mergers across all redshifts we can see that their number reaches a peak around  $z \sim 2$  which coincides with the highest number density of quasars, thus fueling theories that quasars are created during significant merger events in which gas is efficiently supplied to the super massive black hole (Kauffmann and Haehnelt 2000 and references thereafter). Major mergers within the mass range that can be found in

our simulation prove to be an excellent foundation for further analysis.

Two plots linked with formation time of halos give us yet another insight into evolution of halos.

The plot of the highest mass halos within the simulation is explored as a very simple but powerful tool for preliminary analysis of simulation. We can use this method to identify when the first halos of certain mass appear in our simulation which gives us constraints on single halo mass expectations at high redshifts. For example, it shows us that halos of greater mass form the later in the simulation -  $10^{12} M_{\odot}/h$  appear around  $z \sim 6$ , halos of mass of  $10^{13} M_{\odot}/h$  can first be discerned around  $z \sim 4$  etc.

We also investigate a simple derivation of the highest mass halo within a snapshot as a new way for simple preliminary analysis of halo formation during cosmological runs. Modern simulations are becoming bigger (having a large number of particles) involving more data and stressing the need for less costly real time analysis. Deriving the highest mass halo within a snapshot is far less complicated (therefore demanding less resources) than deriving the halo mass function or halo growth function, but can be used as an indication on where those analysis should be of most interest for us. Halo finders are already performing on the fly analysis of simulations making this immediately available analysis. Small jumps in mass in several places on the plot of highest mass halos are obvious markers of significant merger events. Those kind of information is important if the resources are limited and we want to continue our analysis (but without the need for completion of simulation, for example).

Mind due, this analysis can not be used for determining halo mass function or halo formation time. For that we turn to the mean formation time plot (blue triangles, Fig. 4). Number of halos at the final redshift is sufficient to determine mean formation time of halos, in a good agreement with results of other simulations. For example, we notice a good agreement between the empirical fit from Millennium simulation plotted over our results for the same analysis. Figure 4 shows the tendency that higher mass halos form later in the simulation.

From these analysis inference can be made that lower mass halos tend to form earlier and that higher mass halos tend to form later in the simulation. Together with visualization and this analysis we can also derive that a considerable clustering is in progress which, after certain time period, reduces possibility for major merger events, as observed in Fig. 3.

For more details on general halo evolution in a specific mass range and across all redshifts we turn to a more specific analysis, such as the halo mass function and halo growth functions.

One question is how much can different cosmological parameters influence halo mass functions? Jenkins et al. (2001), Warren et al. (2006) and Tinker et al. (2008), amongst others, have tried to address and investigate the issue. Multiplicity function has a universal form, where the same fitting parameters are used as consistent across different cosmologies. Jenkins et al. (2001) found consistency

for different CDM cosmologies up to  $\sim 15\%$ . But within different  $\Lambda$ CDM cosmologies Warren et al. (2006) showed that there is a probable nonnegligible inconsistency while varying several parameters ( $\Omega_m$ ,  $\sigma_8$ ,  $h$ ), where the consistency can be up to 5% for smaller variations. Results of Tinker et al. (2008) confirm that there is an inconsistency, but that it is related to the large variations in cosmologies ( $\Omega_m = 0.1 - 1$ ). They point that the universality below 5% is reachable (and desirable in an era of precision cosmology) but that is an extremely challenging task and beyond the scope of this paper. Considering that all the mass functions referenced here have a similar cosmology (except Press-Schechter one) the consistency between them is sufficient for general comparison.

Looking at halo mass function plots (Fig. 5) where we compare expectations with our data, we see a good agreement with all fits for halos at redshift  $z = 0$ . There is slight underabundance of highest mass halos in our simulation, which is easily explained by small statistical sample populating this bin. A better agreement is easily seen at other redshifts. It is also noticeable that SMT, Warren, and Angulo fits are consistent among themselves. On the other hand, we see that the PS fit is not in a good agreement for the entire mass range and at all redshifts. The smallest discrepancy is at redshift 0, and it gets larger toward earlier redshifts, especially underestimating the number of halos populating higher mass bins. Considering that higher mass halos tend to diverge from sphericity due to violent nature of their formation (mergers, higher density regions, etc), they tend to collapse sooner than PS is estimating, thus slightly increasing their abundance as can be seen both from our simulation and from other fits. Also, as pointed above, different cosmology used for Press-Schechter can also contribute to the observed discrepancy.

If we divert our attention to the halo growth function, unlike in the previous work (Heitmann et al 2006, Lukić et al. 2007), we extend our simulation halo growth function over whole simulation period in which the halos were identified. If we look at Fig. 6, it is immediately clear that all fits diverge at higher redshifts, and this is where we can see the true difference between them. Note that Warren et al. (2006) and Angulo et al. (2012) fits have the highest consistency between them, both being derived purely from numerical simulations, slightly misaligning only at high redshifts. At these redshifts it becomes quite obvious how much PS diverges from other fits.

Interestingly, our simulation follows the SMT fit on lowest mass bin. The highest mass bin is again affected by smaller number of halos populating it although, at redshifts between 0 and 1, all fits and our data converge. On other two remaining (middle) bins, our data follow the Warren fit most consistently. This is expected considering that both Warren simulations and our data suffer from a limited periodic box size, where Warren, during resimulations, had a limited number of realizations of the Universe. Unlike them, Angulo had one sufficiently big box with a superior mass resolution.

Curiously, since the first identification of halos of high masses (more than  $10^{14} M_\odot/h$ ) we have a slight overabundance of them on earlier redshifts as can be seen from the halo growth plot (Fig. 6) but we end up with a slight underabundance of the highest mass halos as can be seen from the mass function for redshift 0 (Fig. 5). It should be duly noted though that their number hasn't reached the plateau as it did for the halos in lower mass bins. It is obvious that mass functions have different crossover times depending on their mass.

As we see, the extending halo growth function makes it possible to continuously monitor the evolution of halo number density within given mass ranges and to qualitatively compare it with fits at higher redshifts, an area of interest which is becoming more and more important in the era of precision cosmology.

From all the analysis combined with halo growth and mass function it is easily deduced, as has been done before, that the most of dark matter halos is migrating from smaller mass halos toward more and more massive halos (as is predicted by “bottom-up” model of CDM - Peebles (1965), Peebles and Dicke (1968), Silk (1968), Gott and Reese (1975), etc.), implying more prominent clustering toward lower redshifts.

Overall, through these analysis, it is seen that our simulation is in a good agreement with analytical and empirical expectations and with previous numerical simulations. The simulation covers evolution of halos over 4 orders of magnitude ( $10^{11} - 10^{15} M_\odot/h$ ) and at redshifts of  $z = 0 - 7$  halos from simulation have a good statistics for halo analysis especially in the mass range of  $10^{11} - 10^{14} M_\odot/h$  and therefore it will be used as a platform in subsequent studies.

*Acknowledgements* – Author would like to thank his mentor Miroslav Mićić for guidance and devoted support during this project. Author would like to thank also Manodeep Sinha for useful advices and discussion. Gratitude goes to him and to Kelly Holley-Bockelmann for help with setting initial conditions. During the work on this paper the author was financially supported by the Ministry of Education and Science of the Republic of Serbia through the project: 176021 ‘Visible and invisible matter in nearby galaxies: theory and observations’.

Numerical results were obtained on the PARADOX cluster at the Scientific Computing Laboratory of the Institute of Physics Belgrade, supported in part by the national research project ON171017, funded by the Serbian Ministry of Education, Science and Technological Development.

## REFERENCES

- Aarseth, S. J.: 1963, *Mon. Not. R. Astron. Soc.*, **126**, 223.
- Angulo, R. E., Hahn, O. and Abel, T.: 2013, *Mon. Not. R. Astron. Soc.*, **434**, 3337.
- Angulo, R. E., Springel, V., White, S. D. M., Jenkins, A., Baugh, C. M. and Frenk, C. S.: 2012, *Mon. Not. R. Astron. Soc.*, **426**, 2046.

- Angulo, R. E., Lacey, C. G., Baugh, C. M. and Frenk, C. S.: 2009, *Mon. Not. R. Astron. Soc.*, **399**, 983.
- Behroozi, P. S., Wechsler, R. H. and Wu, H.-Y.: 2013, *Astrophys. J.*, **762**, 109.
- Behroozi, P. S., Wechsler, R. H., Wu, H.-Y., Busha, M. T., Klypin, A. A. and Primack, J. R.: 2013, *Astrophys. J.*, **763**, 18.
- Bond, J. R., Kofman, L. and Pogosyan, D.: 1996, *Nature*, **380**, 603.
- Boylan-Kolchin, M., Springel, V., White, S. D. M., Jenkins, A. and Lemson, G.: 2009, *Mon. Not. R. Astron. Soc.*, **398**, 1150.
- Bridge, C. R., Carlberg, R. G. and Sullivan, M.: 2009, *Astrophys. J.*, **709**, 1067.
- Bryan, G. L. and Norman, M. L.: 1998, *Astrophys. J.*, **495**, 80.
- Burkey, J. M., Keel, W. C., Windhorst, R. A. and Franklin, B. E.: 1994, *Astrophys. J.*, **429**, L13.
- Colin, P., Avila-Reese, V. and Valenzuela, O.: 2000, *Astrophys. J.*, **542**, 622.
- Cooray, A. and Sheth, R.: 2002, *Physics Reports*, **372**, 1.
- Crocce, M., Pueblas, S. and Scoccimarro, R.: 2006, *Mon. Not. R. Astron. Soc.*, **373**, 369.
- Davis, M., Efstathiou, G., Frenk, C. S. and White, S. D. M.: 1985, *Astrophys. J.*, **292**, 371.
- Dehnen, W. and Read, J. I.: 2011, *The European Physical Journal Plus*, **126**, 55.
- Fakhouri, O. and Ma, C.-P.: 2008, *Mon. Not. R. Astron. Soc.*, **386**, 577.
- Fakhouri, O., Ma, C.-P. and Boylan-Kolchin, M.: 2010, *Mon. Not. R. Astron. Soc.*, **406**, 2267.
- Genel, S., Genzel, R., Bouché, N., Naab, T. and Sternberg, A.: 2009, *Astrophys. J.*, **701**, 2002.
- Gott, J. R., III and Rees, M. J.: 1975, *Astron. Astrophys.*, **45**, 365.
- Gottloeber, S., Klypin, A. and Kravtsov, A. V.: 2001, *Astrophys. J.*, **546**, 223.
- Gottloeber, S., Hoffman, Y. and Yepes, G.: 2010, in Proceedings of High Performance Computing in Science and Engineering, Springer-Verlag, Berlin-Heidelberg.
- Harker, G., Cole, S., Helly, J., Frenk, C. and Jenkins, A.: 2006, *Mon. Not. R. Astron. Soc.*, **367**, 1039.
- Heitmann, K., Lukic, Z., Habib, S. and Ricker, P. M.: 2006, *Astrophys. J.*, **642**, L85.
- Holmberg, E.: 1941, *Astrophys. J.*, **94**, 385.
- Hopkins, P. F., Croton, D., Bundy, K. et al.: 2010, *Astrophys. J.*, **724**, 915.
- Jenkins, A., Frenk, C. S., White, S. D. M., Colberg, J. M., Cole, S., Evrard, A. E., Couchman, H. M. P. and Yoshida, N.: 2001, *Mon. Not. R. Astron. Soc.*, **321**, 372.
- Kauffmann, G., Colberg, J. M.; Diaferio, A. and White, S. D. M.: 1999, *Mon. Not. R. Astron. Soc.*, **307**, 529.
- Kauffmann, G. and Haehnelt, M.: 2000, *Mon. Not. R. Astron. Soc.*, **311**, 576.
- Kauffmann, G. and White, S. D. M.: 1993, *Mon. Not. R. Astron. Soc.*, **261**, 921.
- Kim, J., Park, C., Rossi, G., Lee, S. M. and Gott, J. R. III: 2011, *J. Kor. Astron. Soc.*, **44**, 217.
- Lacey, C. and Cole, S.: 1993, *Mon. Not. R. Astron. Soc.*, **262**, 627.
- Lahav, O. and Liddle, A. R.: 2014, arXiv:1401.1389.
- Le Fevre, O., Abraham, R., Lilly, S. J. et al.: 2000, *Mon. Not. R. Astron. Soc.*, **311**, 565.
- Lukić, Z.: 2008, PhD thesis, Univ. Illinois at Urbana-Champaign.
- Lukić, Z., Heitmann, K., Habib, S., Bashinsky, S. and Ricker, P. M.: 2007, *Astrophys. J.*, **671**, 1160.
- McBride, C., Berlind, A., Scoccimarro, R., Wechsler, R., Busha, M., Gardner, J. and van den Bosch, F.: 2009, *Bulletin of the American Astronomical Society*, **41**, 253.
- Murray, S. G., Power, C. and Robotham, A. S. G.: 2013, *Astronomy and Computing*, **3**, 23.
- Patton, D. R., Pritchett, C. J., Carlberg, R. G., Marzke, R. O., Yee, H. K. C., Hall, P. B., Lin, H., Morris, S. L., Sawicki, M., Shepherd, C. W. and Wirth, G. D.: 2002, *Astrophys. J.*, **565**, 208.
- Peebles, P. J. E.: 1970, *Astron. J.*, **75**, 13.
- Peebles, P. J. E.: 1965, *Astrophys. J.*, **142**, 1317.
- Peebles, P. J. E. and Dicke, R. H.: 1968, *Astrophys. J.*, **154**, 891.
- Planck Collaboration: 2013, arXiv:1303.5062.
- Press, W. H. and Schechter, P.: 1974, *Astrophys. J.*, **187**, 425.
- Seljak, U. and Zaldarriaga, M.: 1996, *Astrophys. J.*, **469**, 437.
- Sheth, R. K., Mo, H. J. and Tormen, G.: 2001, *Mon. Not. R. Astron. Soc.*, **323**, 1.
- Silk, J.: 1968, *Astrophys. J.*, **151**, 459.
- Springel, V.: 2005, *Mon. Not. R. Astron. Soc.*, **364**, 1105.
- Springel, V., Frenk, C. S. and White, S. D. M.: 2006, *Nature*, **440**, 1137.
- Springel, V., White, S. D. M., Jenkins, A. et al.: 2005, *Nature*, **435**, 629.
- Teyssier, R., Pires, S., Prunet, S., Aubert, D., Pichon, C., Amara, A., Benabed, K., Colombi, S., Refregier, A. and Starck, J.-L.: 2009, *Astron. Astrophys.*, **497**, 335.
- Tinker, J., Kravtsov, A. V., Klypin, A., Abazajian, K., Warren, M., Yepes, G., Gottlöber, S. and Holz, D. E.: 2008, *Astrophys. J.*, **688**, 709.
- Vogelsberger, M., Genel, S., Springel, V., Torrey, P., Sijacki, D., Xu, D., Snyder, G., Bird, S., Nelson, D. and Hernquist, L.: 2014, *Nature*, **509**, 177.
- von Hoerner, S.: 1963, *Z. Astrophys.*, **57**, 47.
- Warren, M. S., Abazajian, K., Holz, D. E. and Teodoro, L.: 2006, *Astrophys. J.*, **646**, 881.
- Wetzel, A. R., Cohn, J. D., White, M.: 2009, *Mon. Not. R. Astron. Soc.*, **395**, 1376.
- White, S. D. M.: 1994, astro-ph/9410043.
- White, S. D. M.: 1976, *Mon. Not. R. Astron. Soc.*, **174**, 19.
- White, S. D. M. and Rees, M. J.: 1978, *Mon. Not. R. Astron. Soc.*, **183**, 341.

**СТАТИСТИЧКА АНАЛИЗА РЕЗУЛТАТА КОСМОЛОШКИХ СИМУЛАЦИЈА  
Н ТЕЛА НА СКАЛИ СРЕДЊИХ ЗАПРЕМИНА, ПРИМЕЊЕНА НА ХАЛОЕ**

N. Martinović

*Astronomical Observatory, Volgina 7, 11060 Belgrade 38, Serbia*

E-mail: *nmartinovic@aob.rs*

УДК 524.7–857 : 524.8–17

*Оригинални научни рад*

У овом раду је представљена статистика халоа тамне материје у својству тестирања  $\Lambda CDM$  космолошке симулације N тела (од тренутка формирања првих халоа тамне материје до  $z = 0$ ). Испитујемо нормализован број великих судара у функцији времена, где за функцију времена разматрамо и зависност у функцији црвеног помака и зависност у функцији милијарде година. За потоњу зависност налазимо да је она пропорционална добро познатом степеном закону  $(1 + z)^n$ , где смо добили да је  $n = 2.4$ . Функције масе

халоа и функције раста халоа су добијене и упоређене и са аналитичким и са емпириским фитовима. Функција раста халоа је проширења тако да потпуно обухвата све периоде у симулацији у којима су идентификовани халои тамне материје, омогућавајући да се континуално прати еволуција густине халоа у задатим распонима масе. Визуализација симулације је такође представљена. На црвеним помацима  $z = 0 - 7$  статистика халоа је јако добра за даље анализе, посебно у распону масе од  $10^{11} - 10^{14} M_\odot/h$ .